



# EurJOC

European Journal of Organic Chemistry

 **Chemistry  
Europe**  
European Chemical  
Societies Publishing

## Accepted Article

**Title:** Naphthalene Diimide-Based Molecules for Efficient and Stable Perovskite Solar Cells

**Authors:** Silvia Valero, Andrea Cabrera-Espinoza, Silvia Collavini, Jorge Pascual, Nevena Marinova, Ivet Kosta, and Juan Luis Delgado

This manuscript has been accepted after peer review and appears as an Accepted Article online prior to editing, proofing, and formal publication of the final Version of Record (VoR). This work is currently citable by using the Digital Object Identifier (DOI) given below. The VoR will be published online in Early View as soon as possible and may be different to this Accepted Article as a result of editing. Readers should obtain the VoR from the journal website shown below when it is published to ensure accuracy of information. The authors are responsible for the content of this Accepted Article.

**To be cited as:** *Eur. J. Org. Chem.* 10.1002/ejoc.202000287

**Link to VoR:** <https://doi.org/10.1002/ejoc.202000287>

WILEY-VCH

# Naphthalene Diimide-Based Molecules for Efficient and Stable Perovskite Solar Cells

Silvia Valero,<sup>[a]</sup> Andrea Cabrera-Espinoza,<sup>[a]</sup> Silvia Collavini,<sup>\*[a]</sup> Jorge Pascual,<sup>[b]</sup> Nevena Marinova,<sup>[a]</sup> Ivet Kosta,<sup>[c]</sup> and Juan Luis Delgado<sup>\*[a,d]</sup>

[a] Dr. S. Valero, A. Cabrera-Espinoza, Dr. S. Collavini, Dr. N. Marinova, Prof. J. L. Delgado  
POLYMAT, University of the Basque Country UPV/EHU, Avenida de Tolosa 72 & Faculty of Chemistry, P. Manuel Lardizabal 3, 20018  
Donostia-San Sebastián, Spain  
E-mail: silvia.collavini@polymat.eu, juanluis.delgado@polymat.eu  
<http://www.polymat.eu/en/groups/hybrids-materials-for-photovoltaics>

[b] Dr. Jorge Pascual  
Helmholtz-Zentrum Berlin für Materialien und Energie GmbH,  
Hahn-Meitner-Platz 1, 14109 Berlin, Germany

[c] Dr. I. Kosta  
CIDETEC, Basque Research and Technology Alliance (BRTA), P. Miramón 196, 20014  
Donostia-San Sebastián, Spain

[d] Prof. J. L. Delgado  
Ikerbasque, Basque Foundation for Science,  
Bilbao, Spain

Supporting information for this article is given via a link at the end of the document.

**Abstract:** Naphthalene-diimide (NDI)-based molecules have shown an interesting behaviour within the field of perovskite solar cells, thanks to their promising application as electron transporting materials. In this paper, three novel NDI-containing molecules are synthesized and fully characterized, more specifically two polymers and an analogue small molecule. Each one of the NDI units contains an amine, either ternary or quaternary, which is a moiety known for improving the conductivity. The newly synthesized compounds are suitable for the use as n-type buffer layers on the top of PC<sub>61</sub>BM, thanks to their appropriate energy levels and their solubility in polar solvents. The photovoltaic performances of the NDI-containing cells are highly comparable to those of the reference cells, which contain bathocuproine (BCP) as buffer layer. Furthermore, the stability of the NDI-containing cells is higher than that of the BCP reference.

## Introduction

In the last decade, perovskite solar cells (PSCs) went through a surprisingly fast development, with their power conversion efficiency (PCE) improving from 3.8% to the latest registered value of 25.2%.<sup>[1, 2]</sup> Each one of the components of the perovskite device is under constant and extensive study in order to get the best out of its performances. Together with the other device layers, several charge transporting materials, both organic and inorganic, have been employed during the years.<sup>[3-5]</sup> Among all the structures that have been tested as ETMs, TiO<sub>2</sub> has been widely used and it is still the dominant ETM in PSCs.<sup>[1]</sup> However, it has a major drawback: it requires a high processing temperature (~500 °C), which implies the need of higher costs but also impedes the development of flexible devices.<sup>[6]</sup> Moreover TiO<sub>2</sub> suffers UV instability, leading to the formation of trap states, which can affect both efficiency and stability of PSCs. To overcome these limitations, a variety of ETMs, including inorganic, organic, or polymers, has been tested in the last years.<sup>[7]</sup> Organic semiconductors are easy to prepare and manipulate and their properties can be finely tuned through chemical synthesis.<sup>[3]</sup> Until now, the vast majority of studies concerning

organic ETMs considered fullerene and derivatives for the purpose.<sup>[5, 8]</sup> Their success is due to their excellent properties, such as extremely efficient electron transport, suitable energy alignment with perovskites, stability, and low processing temperature. Moreover, they are well-known for reducing the undesirable phenomenon of hysteresis thanks to their ability to passivate trap states, and they can be processed at low temperatures.<sup>[9]</sup> The most widely used fullerene derivative in solar cells is Phenyl-C<sub>61</sub>-butyric acid methyl ester (PC<sub>61</sub>BM).<sup>[10-12]</sup> It has the tendency to create a charge-transporting network thanks to the phenyl moiety, which is inclined to undergo π-π stacking with other PC<sub>61</sub>BM molecules. The highest occupied molecular orbital (HOMO) and the lowest unoccupied molecular orbital (LUMO) levels of PC<sub>61</sub>BM, which are -5.9 eV and -3.9 eV respectively, make it suitable for extracting electrons and blocking holes coming from methylammonium lead iodide perovskite (CH<sub>3</sub>NH<sub>3</sub>PbI<sub>3</sub>, or MAPbI<sub>3</sub>), whose valence and conduction bands are, respectively, -5.4 eV and -3.9 eV.<sup>[13]</sup> However, PC<sub>61</sub>BM is not flawless. Thickness of PC<sub>61</sub>BM layer is critical: the films made using this molecule are often too thin to completely cover the perovskite, due to the small molecular size of PC<sub>61</sub>BM and the low viscosity of the PC<sub>61</sub>BM solution, which together with the poor solubility of the molecule in the processing solvents could lead to the generation of small cracks in the films.<sup>[14, 15]</sup> These cracks can act as a shunting pass, leading to losses in performance. On the other hand, an excessive thickness confers too high resistivity to the solar cell. Therefore, the morphology and the electrical properties of PC<sub>61</sub>BM-based electron transporting layer (ETL) need to be tuned in order to obtain high-performance PSCs. One efficient way to improve the performances of PC<sub>61</sub>BM is to employ a buffer layer between the fullerene and the metal cathode. The most known buffer layer for PC<sub>61</sub>BM is bathocuproine (BCP).<sup>[11]</sup> In the present work, an ammonium-bearing naphthalene diimide polymer (**P1**) was synthesized, together with its ternary amine polymer counterpart (**P0**) and its small molecule analogue (**M1**) as a comparison. Naphthalene diimides (NDIs) are the smallest component of the family of rylene diimides and consist in a naphthalene core with imide substituents at the 1,4,5,8 positions (Figure 1).<sup>[16]</sup>

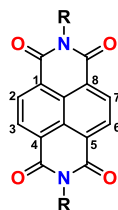


Figure 1: General structure of NDIs.

NDIs are chemically and functionally versatile: their naphthalene core could be substituted at the positions 2, 3, 6, and 7 giving derivatives with variable properties, and the imide unit could be functionalised to modulate the solubility or to tether a specific functional fragment. NDIs are electron-deficient aromatic compounds, due to the strong electron-withdrawing diimide groups. They are planar molecules with the ability to stack both in an intra- and intermolecular arrangement, leading to potential pathways for electron conduction. Moreover, they have good electron mobility, excellent thermal and oxidative stability, and they can be easily solution processed. All these properties, together with their easy and low-cost synthesis make them promising candidates for photovoltaic devices.<sup>[17]</sup> In fact, NDIs have been used several times as ETMs for PSCs with interesting results, both as small molecules<sup>[18-22]</sup> and polymers.<sup>[23-25]</sup>

Regarding the latter, their film-forming property is generally better than that of small molecules, thus providing better processing window for the preparation of high-quality films, based on scalable coating methods. The studies carried out until now have highlighted that one of the features of an ideal NDI polymer is a continuous conjugation, to guarantee good electron mobility and reduce recombination.<sup>[25]</sup>

Last but not least, NDI-based ETLs have demonstrated to be cheaper than the reference ETL, PC<sub>61</sub>BM.<sup>[26]</sup>

The novel molecules chosen for this study were incorporated as buffer layers in order to improve the performances of PC<sub>61</sub>BM. The high polarity of these novel compounds make them suitable for the purpose, with no risk of dissolving the underlying PC<sub>61</sub>BM layer during deposition. To the best of our knowledge, this is the first time the potential of these useful structures is used to improve the performances of the well-known PC<sub>61</sub>BM. The performances of the NDI-containing devices were compared to those of a cell containing BCP, as a reference. To conclude this study, the stability of the cells was evaluated.

## Results and Discussion

### Syntheses of the Target Compounds

The structure of the target compounds **P0**, **P1**, and **M1** is reported in Figure 2. The backbone of polymers **P0** and **P1** is composed of a benzene unit combined with different NDI-based moieties. The benzene unit connected to the 2, 6-positions of the NDI core should help obtain a more extended conjugation than the one that would be generated through the bonding of the sterically hindered NDI positions. Furthermore, to ensure sufficiently high solubility for device fabrication and good film formation, branched alkyl chains (2-ethylhexyl) were introduced in the benzene unit. Polymers **P0** and **P1** hold respectively an amino- or an ammonium-functionalized side chain at the imide positions of the NDI core. It has been proven that both amino or

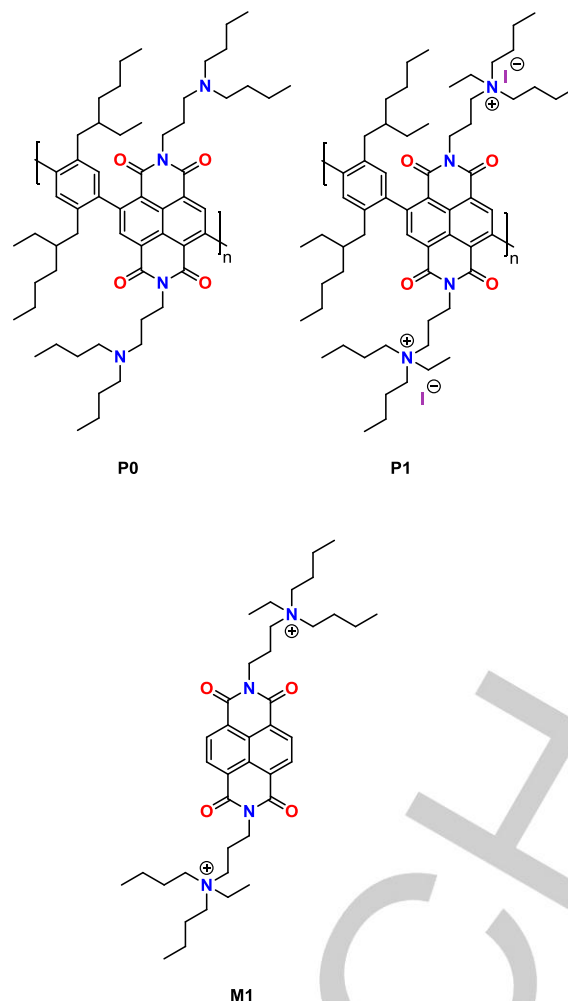


Figure 2: Structure of the target compounds **P0**, **P1**, and **M1**.

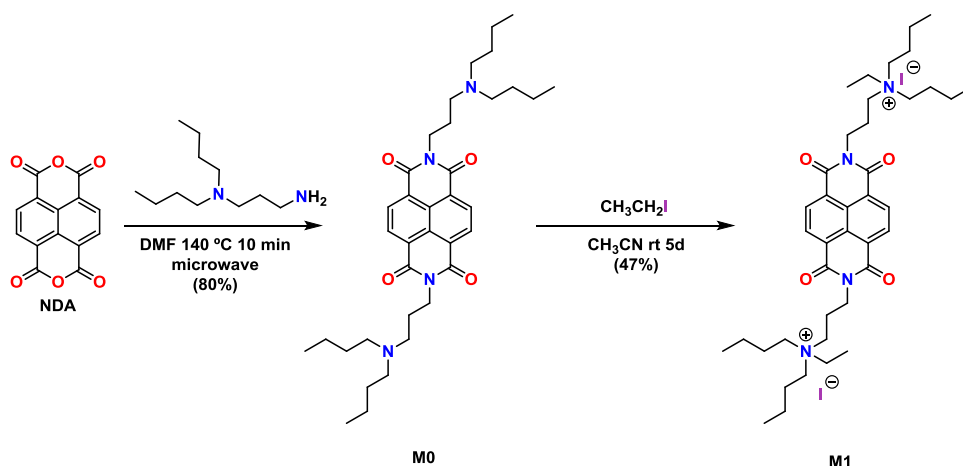
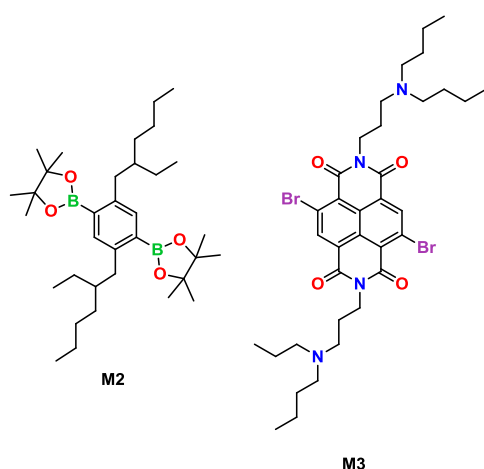
quaternary ammonium halides can effectively passivate trap states in perovskites, with consequent reduction of the charge recombination and improvement of the charge extraction at the perovskite/ETM interface.<sup>[25, 27]</sup>

In addition, both tertiary and quaternary ammonium groups improve the conductivity of polymeric n-type organic semiconductors.<sup>[28]</sup> More specifically, regarding the quaternary ammonium, as an immediate consequence the halogen anions contribute to transfer electrons to the ETL, increasing its conductivity and therefore the short-circuit current density ( $J_{sc}$ ) of the cell. Furthermore, the presence of a tertiary amine in most of the doping agents induces self-doping of the layer, thanks to the lone pair electron transfer to the ETL.<sup>[29]</sup>

To determine the role of the polymeric nature of the molecule, a small molecule bearing the same chain as **P1**, named **M1**, was synthesized. The synthesis of **M1** is reported in Scheme 1.

To obtain molecule **M1**, the commercially-available 1,4,4,8-naphthalenetetracarboxylic dianhydride (NDA) was treated with 3-(dibutylamino)propylamine in dimethylformamide (DMF) at 140 °C under microwave irradiation to get molecule **M0**. This was then treated with iodoethane in CH<sub>3</sub>CN at room temperature in the absence of light for 5 days.

The preparation of polymers **P0** and **P1** started with the synthesis of the monomers **M2** and **M3**, depicted in Figure 3. These monomers are engineered to be the proper reagents for

Scheme 1: Synthetic pathway to molecule **M1**.Figure 3: Structures of the monomers **M2** and **M3**

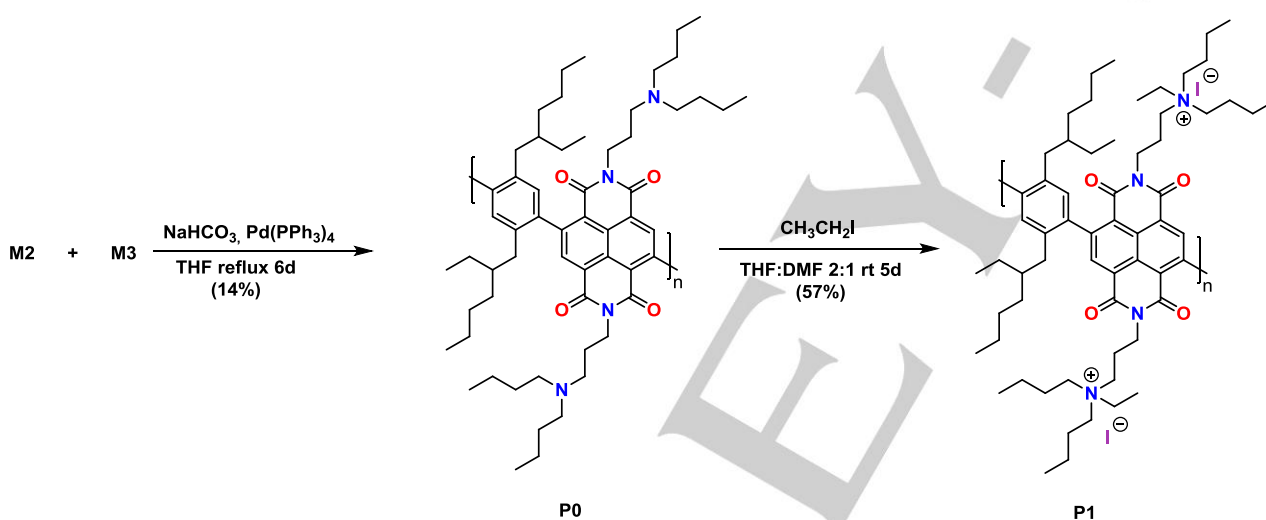
the subsequent Pd-catalyzed Suzuki cross coupling reactions that allowed the obtaining of the polymers. The synthetic strategy to prepare monomer **M2** is shown in Scheme S1. First, the Kumada coupling of 3,4-dibromobenzene with 2-(ethylhexyl)magnesiumbromide (RMgBr) provided 1,4-bis(2-

ethylhexyl)benzene (**M4**), which was brominated leading to compound **M5**, which after a Miyaura borylation gave monomer **M2**.

The synthesis of monomer **M3** is shown in Scheme S2. The preparation of intermediate **M6** was necessary, and it was carried out following a reported procedure.<sup>[30]</sup> The reaction between NDA and 1,3-dibromo-5,5-dimethylhydantoin (DBDMH) in H<sub>2</sub>SO<sub>4</sub> gave intermediate **M6**, which was then imidated with 3-(dibutylamino)propylamine in acetic acid (AcOH) leading to monomer **M3**.

The synthesis of polymer **P0** was performed through Pd-catalyzed Suzuki coupling copolymerization of the diboronate ester monomer **M2** with the NDI-based monomer **M3** in THF using NaHCO<sub>3</sub> as base (Scheme 2). The resulting mixture was purified through Soxhlet extraction in MeOH, CH<sub>3</sub>CN and acetone giving polymer **P0** as a product. Polymer **P1** was then obtained by quaternizing the precursor polymer **P0** with an excess of iodoethane in a mixture of DMF:THF solution at room temperature in darkness for 5 days. Both syntheses are reported in Scheme 2.

The fully detailed syntheses of all compounds can be found in the Experimental Section.

Scheme 2: Syntheses of polymers **P0** and **P1**

### Characterization of the target compounds

The chemical structure of both polymers **P0** and **P1** were confirmed by  $^1\text{H-NMR}$  spectroscopy. Moreover, through the mass spectrometry analysis of **P0**, it was possible to find peaks which differ from each other by a value that corresponds to the building block ( $m/z$  calculated for  $[\text{C}_{58}\text{H}_{86}\text{N}_4\text{O}_4]^+$ : 902.664), as shown in Figure 4.

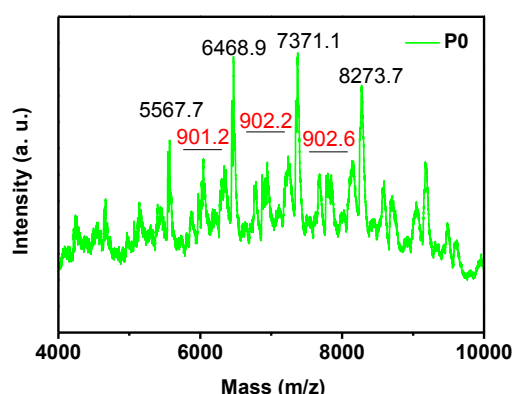


Figure 4. MALDI-TOF of polymer **P0**.

Polymer **P1** could not be analyzed by MALDI-TOF, most likely due to the difficulty of polycationic polymers to be ionized.<sup>[31]</sup>

Figure 5 shows the  $^1\text{H-NMR}$  spectra of polymers **P0** and **P1**. It can be observed how the signal between 2.20-2.70 ppm (highlighted in blue) attributed to the hydrogen atoms closer to the amine in polymer **P0**, is shifted between 2.80-3.74 ppm in polymer **P1**, due to the deshielding effect produced by the protonated amine. Moreover, in that region another signal appeared, which is assigned to the proton close to the quaternized amine ( $-\text{NCH}_2\text{CH}_3$ ) in polymer **P1**. These are strong evidences of the conversion of polymer **P0** into polymer **P1**.

The molecular weight of polymers **P0** was estimated by size-exclusion chromatography (SEC) analysis in THF compared to a polystyrene standard (Table 1). It showed a  $M_n$  value of  $4350\text{ g mol}^{-1}$ , leading to  $X_n$  values of 5. These values were comparable to those obtained for other NDI-based polymers described in literature.<sup>[32-36]</sup> Polymer **P1** could not be analyzed through SEC due to its insolubility in THF. However, it is safe to assume that polymer **P1** would have a molecular weight of the same order as that of its neutral precursor **P0**. This assumption is based on the process used to obtain **P1**, which only implies the use of iodoethane without resorting to further polymerization processes.

Table 1. Molecular weights of polymer **P0**.

	$M_n$ ( $\text{g mol}^{-1}$ )	$M_w$ ( $\text{g mol}^{-1}$ )	$X_n$	PDI
<b>P0</b>	4350	6953	5	1.60

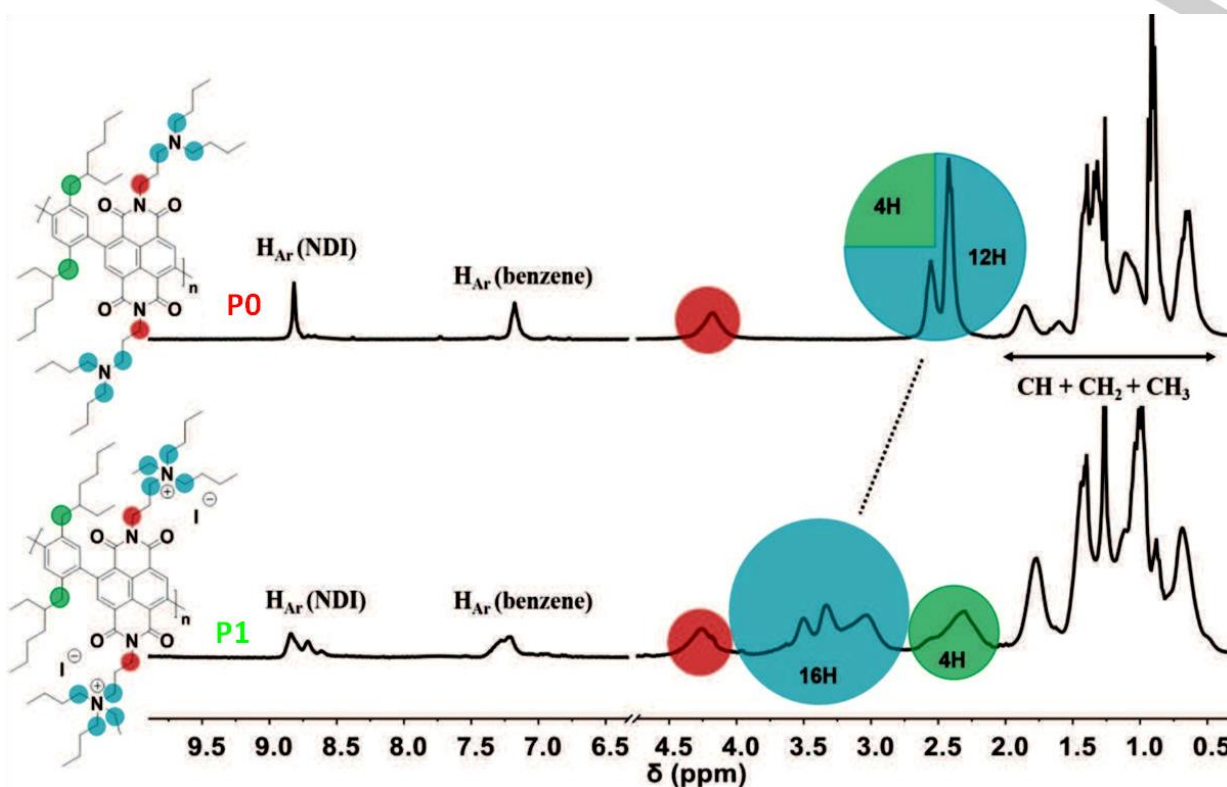


Figure 5.  $^1\text{H-NMR}$  spectra (300 MHz,  $\text{CD}_2\text{Cl}_2$ , 298 K) of polymers **P0** (top) and **P1** (bottom).

### Optical properties

The optical properties of the compounds were inspected resorting to UV-Vis absorption measurements. Figure S1 shows

the absorption spectrum of **M1** recorded in DCM. As it can be seen, the compound shows two intense absorption bands below 400 nm attributed to the  $\pi-\pi^*$  transition (Table S1).<sup>[37]</sup> The

bandgap value could be estimated from the absorption onset of the longest absorption wavelength and is as well reported in Table S1.

The absorption spectra of polymers **P0** and **P1** in DCM are depicted in Figure S2. The registered data are reported in Table S2. The polymers displayed very low absorption in the visible range, which is a favourable feature for their application in perovskite-based devices. Both polymers exhibit a similar absorption pattern with four distinct absorption bands. A broad peak lies at the low-energy region (400-520 nm) and is related to an intramolecular charge transfer (ICT) process between the electron donor (benzene) and the NDI electron-deficient unit, which was in accordance with previously reported NDI-donor copolymers.<sup>[38-41]</sup> The ICT absorption peak of the ammonium-functionalized copolymer **P1** is slightly red-shifted compared to that of **P0**, which could be due to the electrostatic perturbation given by ions in close proximity to the optically active segment, solvatochromic effects arising from the polar solvent, or multichain aggregation.<sup>[28]</sup> The other three absorption bands lie in the high-energy region (249-380 nm) and can be assigned to  $\pi$ - $\pi^*$  transitions of the backbones. Among these, the absorption band centred in between 249 and 253 nm is the most intense and can be assigned to  $\pi$ - $\pi^*$  transitions of the benzene unit. The other two absorption bands are characteristics of  $\pi$ - $\pi^*$  transitions of the NDI core, similar to those registered for the small molecule **M1**.

### Electrochemical properties

The electrochemical properties of the compounds were investigated by Cyclic Voltammetry (CV) measurements, which were carried out in a 0.1 M solution of tetra-*n*-butylammonium fluoride (TBAHFP) in anhydrous DCM. The LUMO values (Table 2 and 3) were obtained from the half-wave potential of the first reduction ( $E_{1/2}^{\text{Red1}}$ ) during CV measurements using the Fc/Fc<sup>+</sup> redox couple as the internal standard. Therefore, the LUMO is calculated according to the following equation:

$$\text{LUMO (eV)} = -4.8 - E_{1/2}^{\text{Red1}}$$

**M1** underwent two reversible reduction processes, which indicated an initial radical anion and subsequent dianion formation and are typical of the NDI derivatives (Figure 6).<sup>[35]</sup>

The low LUMO value registered for molecule **M1** could be due to anion- $\pi$  interactions between the electron deficient aromatic NDI core and the I<sup>-</sup> anions.<sup>[42, 43]</sup> In addition, **M1** suffered two oxidation processes, which were non-reversible.

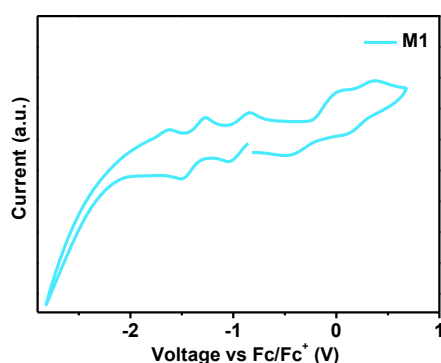


**Figure 6.** Cyclic voltammogram of model compound **M1** in DCM/TBAHFP (0.1 M) at a scan rate of 100 mV s<sup>-1</sup>.

**Table 2:** Electrochemical properties and energy levels of compound **M1**. All the values are expressed in eV.

	$E_{1/2}^{\text{Red1}}$	LUMO	Bandgap	HOMO
<b>M1</b>	-0.94	-3.86	3.14	-7.00

Similar to what registered for the small molecule, the novel polymers show two reversible reduction processes, due to the NDI core (Figure 7). Also in this case, the LUMO value of the ammonium-containing polymer **P1** is lower than that of the neutral counterpart, and again it could be explained with the anion  $\pi$ -interactions between the NDI and the iodine anions. **P1**, similarly to **M1**, suffered two non-reversible oxidation processes, while polymer **P0** does not exhibit any oxidation. This effect could be explained by the lone pair electrons on the nitrogen atom and its tendency to transfer onto the electron-deficient NDIs and to lead to the formation of charge transfer complexes, which was also observed in previous reports.<sup>[28, 44]</sup>

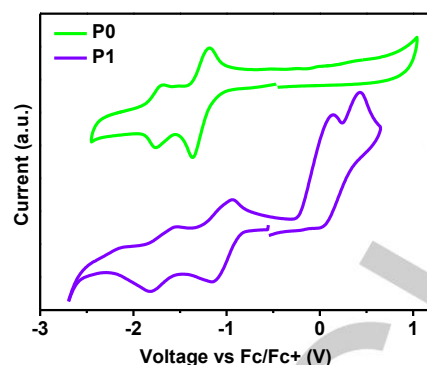


**Figure 7.** Cyclic voltammograms of polymers **P0** and **P1** in DCM/TBAHFP (0.1 M) at a scan rate of 100 mV s<sup>-1</sup>.

**Table 3.** Electrochemical properties and energy levels of polymers **P0** and **P1**. All the values are expressed in eV.

	$E_{1/2}^{\text{Red1}}$	LUMO	Bandgap	HOMO
<b>P0</b>	-1.27	-3.53	2.41	-5.94
<b>P1</b>	-1.05	-3.75	2.35	-6.10

Figure 8 summarizes the energy levels of all the compounds used in the device fabrication.<sup>[45]</sup> With respect to **M1**, the energy levels are highly similar to those of the reference buffer layer BCP, therefore the performances obtained with this molecule are expected to be comparable to the reference. With these LUMO values (summarized in Table 2 and 3), these novel NDI-based small molecules and polymers are compatibles to be used as buffer layers between the PC<sub>61</sub>BM ETL and the gold cathode in inverted PSCs. Hence, these materials can behave as suitable filters towards electrons, which is fundamental for their synergetic action as buffer layer for PC<sub>61</sub>BM. On the contrary, the hole-blocking synergetic action of the polymers is expected to be weaker than those of BCP and **M1**, since their higher-lying HOMOs. Furthermore, **P0** is expected to behave slightly worse than **P1** due to both the higher LUMO and HOMO. Nonetheless, the energy levels might be overall suitable for their application in PSCs and highly compatible with PC<sub>61</sub>BM.

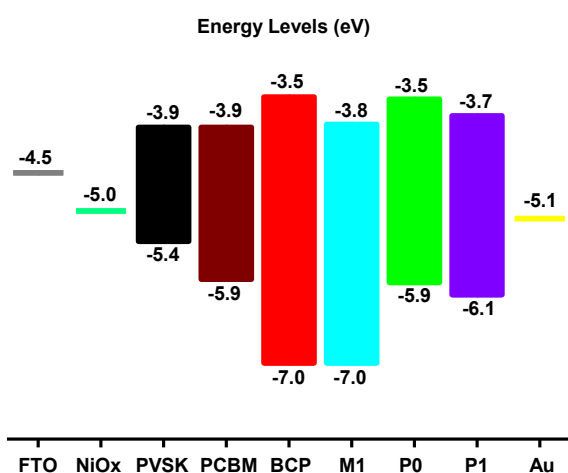


**Figure 8.** Summary of the energy levels of the different compounds considered in the study.

### Thermal properties

To better evaluate their suitability for an application in perovskite device, the thermal behaviour of polymers **P0** and **P1** is investigated by means of TGA and DSC analyses. The thermograms of these copolymers are showed in Figure S3A. Both polymers show thermal stability under operation temperature of PSCs; in fact their Td values, which correspond to their 2% weight losses, are, respectively, 240.20 °C and 188.34 °C. The main decomposition process of copolymer **P0** could be related to the loss of the amino groups. In case of polymer **P1**, the first mass loss was attributed to the loss of the ethyl iodide groups, followed by the loss of the amino groups similarly to what happens to **P0**. Thereafter, both **P0** and **P1** undergo the second major degradation process owing to the

split of the alkyl chains. This trend in the thermal properties was also observed in other conjugated polymers with terminal amino or ammonium side groups.<sup>[28, 46, 47]</sup>

The melting point molecule **M1** was registered in order to get a comparison with the polymers. The observed value was 218 °C, quite higher than the operational temperature of the devices. On the contrary, the melting point of molecule **M0** was observed to be sensibly lower (89 °C).

DSC measurements of **P0** revealed its amorphous nature, showing a Tg values at 157.15 °C. On the contrary, polymer **P1** did not show any thermal feature in the second heating cycle over the temperature range of 25-180 °C (Figure S3B, Table S3).

### Incorporation into PSCs

As stated before, thanks to their solubility, the three novel molecules could be incorporated as buffer layers between the ETL and the gold electrode. The cells were then characterized in terms of performances and their stability was preliminarily evaluated.

The chosen devices architecture was the inverted one: FTO glass/NiOx/CH<sub>3</sub>NH<sub>3</sub>PbI<sub>3</sub>/PC<sub>61</sub>BM/buffer layer/Au. The buffer layer could be either one of the novel molecules (**P0**, **M1**, **P1**) or BCP as a reference. An additional reference was given by preparing devices with no buffer layer, so that PC<sub>61</sub>BM directly contacts with the gold cathode. Further details about the preparation of the cells are reported in the Experimental Section. The statistics of the photovoltaic parameters extracted from the cells, such as J<sub>sc</sub>, open-circuit voltage (V<sub>oc</sub>), fill factor (FF), and PCE, are reported in Figure 9. The best curves of each condition, with the corresponding parameters, are reported in Figure S4. EQE experiments are reported in figure S5 and the photovoltaic parameters extracted from both these experiments and the best curves are reported in table S4

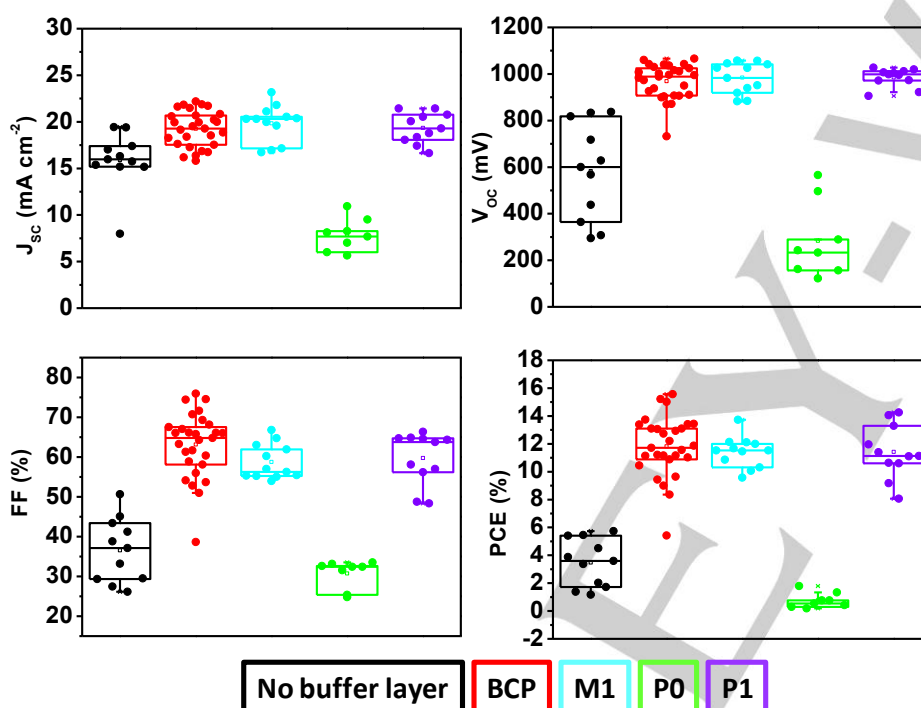


**Figure 9:** Statistics of the photovoltaic parameters (short-circuit current J<sub>sc</sub>, open-circuit voltage V<sub>oc</sub>, fill factor FF, and power conversion efficiency PCE) of the different NDI-containing devices and their references.

**Table 4:** Best and Average photovoltaic parameters of the different NDI-containing devices and their references.

		$J_{sc}$ (mA cm <sup>-2</sup> )	$V_{oc}$ (mV)	FF (%)	PCE (%)
No Buffer Layer	Best	15.2	837	45	5.73
	Average	15.9	583	37	3.48
BCP	Best	21.6	1066	68	15.57
	Average	19.3	969	63	11.82
M1	Best	21.8	1045	60	13.73
	Average	19.8	984	59	11.42
P0	Best	9.5	566	33	1.79
	Average	7.9	284	31	0.76
P1	Best	21.4	1027	65	14.25
	Average	19.4	985	60	11.43

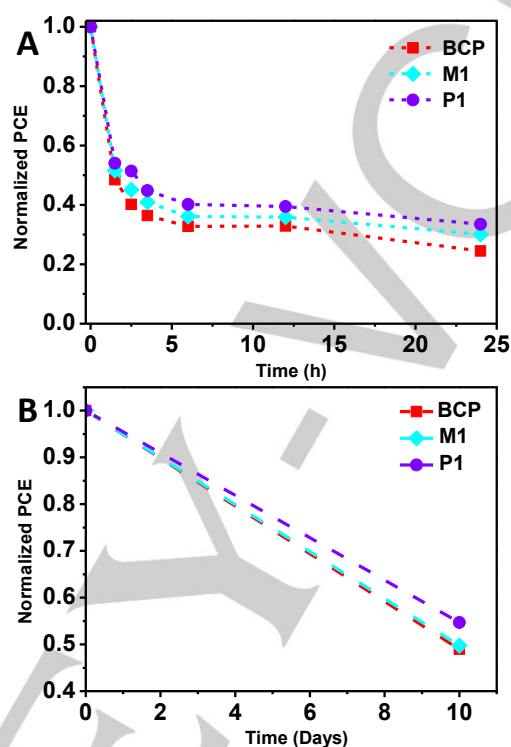
The most important information that could be extracted from these statistics is that the results that were obtained with molecule **M1** and polymer **P1** are highly comparable to those obtained with the reference BCP buffer layer. As a matter of fact, BCP gave an average 11.82% PCE and both **M1** and **P1** gave, respectively, average values of 11.42% and 11.43%. This demonstrates once again the great potential of halogen-ammonium salts for the improvement of the performances of the perovskite devices. The improvement of  $J_{sc}$  led by the novel structure is clear for the case of **M1**, where the average current increases from 19.3 mA cm<sup>-2</sup> of registered with BCP to 19.8 mA cm<sup>-2</sup>. This is confirmed by the results reported in Table 4, which shows both the best and the average photovoltaic parameters. On the contrary, the performances given by **P0** as buffer layer were not satisfactory. The morphology of the devices was studied in order to find out the reason of these lower performances. The FESEM images of the layers are shown in Figure S6. The pinholes of the **P0** layer, which can be observed in the FESEM top view, could have explained the bad results, nevertheless they can be seen also in the case of **P1** even if to a slightly lesser extent, and so this hypothesis has to be rejected. On the contrary, **M1** presented a continuous layer. The thickness of the layers was also investigated, as reported in Figure S7. The layers are sometimes too thin to be differentiated from PC<sub>61</sub>BM, therefore the thicknesses were calculated from the difference between the measured overall ETL and the bare PC<sub>61</sub>BM, which was estimated to be of an average value of 31 ± 4 nm. The obtained thicknesses are reported in Table 5. The standard error was calculated dividing the standard deviation by the square root of the data sample size. The estimated average thickness of P0 is in fact about half of the average thickness measured for the other compounds, and this might be the reason of its lower performances. Due to its poorer performance, **P0** was not further considered for stability tests.

**Table 5:** Estimated average thicknesses of the buffer layers. The standard error was calculated dividing the standard deviation by the square root of the data sample size.

	PCBM+Buffer Layer	Estimated Buffer Layer
	(nm)	Thickness (nm)
BCP	53±6	22
M1	54±2	23
P0	42±7	11
P1	51±9	20

The stability was evaluated in two different ways. The first trial was performed leaving the cells on a hotplate at 80 °C and keeping track of the performances (Figure 10A). In both cases the NDI-containing cells showed higher stability than the reference; the better results obtained with **P1** should be ascribed to the polymeric nature of the compound and its consequent tendency to generate better layers.

The second trial was performed leaving the cells in a dark drawer for a prolonged period of time, in order to evaluate their resistance to air (Figure 10B). In this case, only **P1** could give better results than the reference after 10 days. Its polymeric nature must be once again at the root of this improved stability.

**Figure 10:** A) Normalized PCE of the cells that underwent thermal stability test and B) Normalized PCE of the cells that underwent long-term stability test.

## Conclusions

In summary, three novel n-type NDI-based molecules, **M1**, **P0**, and **P1**, bearing ternary or quaternary ammonium moieties, were designed and synthesized. The compounds were successfully purified as confirmed by a full characterization through different spectroscopic techniques. The analysis of the electrochemical properties of the novel molecules shows that they meet the requirements to be used as buffer layers for the ETL in PSCs. In fact, the compounds showed suitable energy levels with low-lying LUMO levels of about -4 eV and HOMO levels around -6 eV or lower, which would ensure synergetic action with PC<sub>61</sub>BM. Moreover, thermal analysis indicated that polymers are thermally stable with no phase transition under operation temperatures of PSCs. The choice of using them as buffer layers for the ETL finds its root in their proper solubility in polar solvents, which provides an easy processing. The introduction of these molecules into PSCs gave similar results to those obtained with the reference buffer layer, BCP, both in terms of photovoltaic performances and stability. Hence, we could conclude that NDIs are a very promising candidate to improve the performances of PSCs.

## Experimental Section

### Methods and Materials

All commercially available reagents and solvents for synthesis and photovoltaic study were used as received without further purification. Anhydrous solvents were dried using a SPS purification system. Column chromatography was carried out using silica gel (40 to 60 μm, 60 Å) as stationary phase. Thin layer chromatography (TLC) was performed on precoated silica gel and observed under UV light. The <sup>1</sup>H-NMR and <sup>13</sup>C-NMR spectra were taken on Bruker NMR spectrometers (300 MHz for <sup>1</sup>H NMR, 75 MHz and 100 MHz for <sup>13</sup>C NMR) at room temperature. Chemical shifts (δ) are reported in ppm. Abbreviations of coupling patterns are as follows: s = singlet, d = doublet, t = triplet, m = multiplet. Matrix Assisted Laser Desorption Ionization (MALDI) experiments, coupled to a Time-of-flight (TOF) analyzer, were recorded on Bruker REFLEX spectrometer. Electrospray ionization (ESI) measurements were carried out on HPLC Agilent 1200 Series system coupled to a hybrid quadrupole-time of flight (LC-QTOF) mass spectrometer Agilent 6520 from Agilent Technologies (Santa Clara, CA, USA). The molecular weight distribution of the polymers was determined by size exclusion chromatography (SEC, Waters). The setting consisted of a pump, a differential refractometer (Waters 2410) and three columns in series (Styragel HR2, HR4 and HR6; with a pore size from 102 to 106 Å). The analyses were performed at 35 °C and THF was used as solvent at a flow rate of 1 mL min<sup>-1</sup>. Calibration was relative to polystyrene standards. A series of polystyrene standards in the range of 580-3,848,000 g mol<sup>-1</sup> were used to prepare a universal calibration curve. The thermogravimetric analysis (TGA) was performed on a TA Q500 using a 10 °C min<sup>-1</sup> heating rate under a nitrogen flow. Differential scanning calorimetry (DSC) was performed on a DSC3+ Mettler Toledo at a scan rate of 20 °C min<sup>-1</sup> in the nitrogen atmosphere. Absorption measurements were recorded on a Perkin-Elmer Lambda 950 spectrometer. All the compounds were measured at various concentrations (10<sup>-5</sup>-10<sup>-7</sup> mol l<sup>-1</sup>) to affirm linear behaviour. The measurements of films of compounds were performed on samples that were spin-coated from the respective solvent onto FTO/SnO<sub>2</sub> substrates. The optical band gap was estimated from the onset of the absorption edge (λ<sub>onset</sub>) in the longer wavelength region. Cyclic voltammograms were carried out on a Princeton Applied Research Parstat 2273 in a 3-electrode single compartment cell with carbon disc

working electrode, a platinum wire counter electrode and a silver wire pseudoreference electrode. All the potential values were reported versus the redox potential of the ferrocene/ferrocenium redox couple. HOMO and LUMO values were obtained from the onset potentials of cyclic voltammetry measurements. The potential of Fc/Fc<sup>+</sup> is 0.2 V vs. the normal hydrogen electrode (NHE), which has an absolute potential of -4.6 eV vs. vacuum.<sup>[48]</sup> Therefore, the energy levels are HOMO/LUMO (eV) = -4.8 - E<sub>1/2</sub><sup>Ox1/Red1</sup> and the optical band gap = LUMO - HOMO. The morphologies of the films were analyzed with an ULTRA plus ZEISS field-emission scanning electron microscope (FESEM). The absorbance spectra were obtained from the transmittance and reflectance spectra, which were measured with a JASCO V-570 spectrophotometer with an integrating sphere. The J-V characteristics were measured using a 450 W xenon light source (Oriol). The light intensity was calibrated with a Si photodiode equipped with an IR-cutoff filter (KG3, Schott) and it was recorded during each measurement. Current-voltage characteristics of the cells were obtained by applying an external voltage bias while measuring the current response with a digital source meter (Keithley 2400). The voltage scan rate was 20 mV s<sup>-1</sup>, and no device preconditioning was applied before starting the measurement, such as light soaking or forward voltage bias applied for a long time. The cells were masked with a black metal mask of 0.16 cm<sup>2</sup> to estimate the active area and reduce the influence of the scattered light. The external quantum efficiency (EQE) was measured as a function of wavelength from 300 to 850 nm with a step of 10 nm using a home-built small-spot EQE system. A Stanford Research SR830 Lock-In amplifier is used to measure the electrical response of the device under test and evaluated in TracQ-Basic software.

### Synthetic Procedures

**M0**: 1,4,5,8-Naphthalenetetracarboxylic dianhydride (500 mg, 1.87 mmol) was suspended in 5 mL of DMF together with 3-(dibutylamino)propylamine (834 μL, 3.70 mmol). The mixture was left to react under microwave at 140 °C for 10 min. The reaction mixture was then poured into 500 mL of water and the precipitate was filtered off, washed 3 times with water and dried under reduced pressure. The product was kept in darkness (900 mg, 80%).  
<sup>1</sup>H-NMR (300 MHz, CDCl<sub>3</sub>), δ (ppm): 8.75 (s, 4H), 4.22 (t, 4H), 2.58 (t, 4H, 4H), 2.41 (t, 8H), 1.97-1.82 (4H), 1.47-1.22 (16H), 0.89 (t, 12H).  
<sup>13</sup>C-NMR (75 MHz, CDCl<sub>3</sub>), δ (ppm): 162.96, 131.02, 126.81, 126.78, 53.82, 51.94, 39.86, 29.38, 25.71, 20.86, 14.20.  
MS (ESI-TOF): calculated for C<sub>36</sub>H<sub>52</sub>N<sub>4</sub>O<sub>4</sub> [M+H]<sup>+</sup>: 605.406, found: 605.406.  
**M1**: M0 (400 mg, 661 μmol) was dissolved in 2 mL of CH<sub>3</sub>CN and placed in a closed tube under nitrogen atmosphere. After that, iodoethane (3.00 mL, 37.5 mmol) was added to the solution. The mixture was allowed to react at room temperature at dark for 5 d. The product, which precipitates as orange crystals, was collected by filtration, washed several times with Et<sub>2</sub>O and dried over vacuum. The solid was recrystallized from DCM to obtain 310 mg of M1 (47% yield).  
<sup>1</sup>H-NMR (300 MHz, DMSO), δ (ppm): 8.74 (s, 4H), 4.15 (t, 4H), 3.33-3.22 (8H), 3.22-3.10 (8H), 2.15-2.01 (4H), 1.64-1.50 (8H), 1.37-1.22 (8H), 1.18 (t, 6H), 0.91 (t, 12H).  
<sup>13</sup>C-NMR (75 MHz, DMSO), δ (ppm): 162.91, 130.53, 126.42, 126.25, 57.16, 55.02, 53.42, 37.53, 23.07, 20.31, 19.16, 13.49, 7.38.  
MS (ESI-TOF): calculated for C<sub>40</sub>H<sub>62</sub>N<sub>4</sub>O<sub>4</sub> [M]<sup>+</sup>: 662.477, found: 662.476.  
**M2**: 1,4-Dibromo-2,5-bis(2-ethylhexyl)benzene (13, 240 mg, 521 μmol), bis(pinacolato)diboron (389 mg, 1.53 mmol) and potassium acetate (400 mg, 4.08 mmol) were dissolved in 8 mL of anhydrous 1,4-dioxane. The resulting suspension was degassed with an argon stream before and after the addition of PdCl<sub>2</sub>(dppf) (11.0 mg, 15.3 μmol), and the mixture was stirred at 80 °C for 3 d. After cooling down to room temperature, 40 mL of water were added and the aqueous phase was extracted with DCM (2 x 40 mL). The combined organic phases were washed with water (2 x 150 mL), brine (1 x 50 mL) and then dried over anhydrous Na<sub>2</sub>SO<sub>4</sub>, concentrated under reduced pressure and purified by flash column chromatography using hexane:AcOEt (20:1) as eluent to give monomer M2 as a white solid (249 mg, 84%).

<sup>1</sup>H-NMR (300 MHz, CDCl<sub>3</sub>),  $\delta$  (ppm): 7.48 (s, 2H), 2.85-2.70 (4H), 1.59-1.45 (2H), 1.38-1.11 (40H), 0.91-0.77 (12H).

<sup>13</sup>C-NMR (75 MHz, CDCl<sub>3</sub>),  $\delta$ : 144.73, 137.61, 83.41, 42.03, 39.56, 32.02, 28.63, 25.48, 25.00, 23.35, 14.30, 10.84.

MS (MALDI-TOF): calculated for C<sub>34</sub>H<sub>60</sub>B<sub>2</sub>NaO<sub>4</sub> [M+Na]<sup>+</sup>: 577.462, found: 577.459.

**M3:** To a solution of 2,6-dibromo-1,4,5,8-naphthalenetetracarboxylic dianhydride (M9, 500 mg, 1.17 mmol) in 15 mL of AcOH, 3-(dibutylamino)propylamine (660  $\mu$ L, 2.92 mmol) was added slowly at room temperature and stirred at 130 °C for 45 min. Upon completion, the reaction mixture was poured into cooled water and the aqueous phase was neutralized with Na<sub>2</sub>CO<sub>3</sub> and extracted with chloroform until no color could be seen in the organic phase. The combined organic extracts were washed with brine, dried over Na<sub>2</sub>SO<sub>4</sub>, filtered and the solvent removed under reduced pressure. The crude product was purified by flash column chromatography using the mixture CHCl<sub>3</sub>:EtOH (95:5) with 0.5% of NEt<sub>3</sub> as eluent to yield the product (200 mg, 23%).

<sup>1</sup>H-NMR (300 MHz, CDCl<sub>3</sub>),  $\delta$  (ppm): 8.99 (s, 2H), 4.28-4.18 (4H), 2.58 (t, 4H), 2.40 (t, 8H), 1.95-1.81 (4H), 1.46-1.21 (16H), 0.90 (t, 12H).

<sup>13</sup>C-NMR (100 MHz, CDCl<sub>3</sub>),  $\delta$  (ppm): 160.87, 160.85, 139.14, 128.41, 127.82, 125.49, 124.23, 53.77, 51.89, 40.45, 29.27, 25.41, 20.85, 14.28.

MS (MALDI-TOF) calculated for C<sub>36</sub>H<sub>51</sub>Br<sub>2</sub>N<sub>4</sub>O<sub>4</sub> [M+H]<sup>+</sup>: 761.228, found: 761.202.

**M4:** [49] This product was prepared in two steps: (1) preparation of the Grignard reagent (RMgX); (2) the reaction of RMgX with 1,4-dibromobenzene by Kumada coupling.

1) Grignard reaction. To a solution of magnesium (1.65 g, 67.8 mmol) in 4 mL of anhydrous Et<sub>2</sub>O was added one crystal of iodine and 2-ethylhexyl bromide (9.82 g, 50.9 mmol) together with 4 mL of anhydrous Et<sub>2</sub>O slowly (30 min). The mixture was refluxed under argon atmosphere for 1 h.

2) Kumada reaction. To an ice-cooled solution of 1,4-dibromobenzene (4.00 g, 16.9 mmol) and Ni(dppp)Cl<sub>2</sub> (279 mg, 514  $\mu$ mol) in 5 mL of anhydrous Et<sub>2</sub>O was added slowly the Grignard reagent (previously synthesized) together with 5 mL of Et<sub>2</sub>O to transfer that reagent completely. The reaction mixture was stirred at 40 °C under argon atmosphere during 2 d. After this time, 50 mL of HCl (1 M) was added to the reaction mixture and the aqueous phase was extracted with Et<sub>2</sub>O (3 x 50 mL). The combined organic phases were washed with water (2 x 150 mL) and brine (1 x 150 mL), dried over Na<sub>2</sub>SO<sub>4</sub> and concentrated under reduced pressure. The resulting yellowish oil was purified by vacuum distillation (43 mbar, 200 °C) to give a colorless oil (3.82 g, 74%), which was used directly in the next step without further purification.

This compound was previously described in literature and showed identical spectroscopic data as those reported therein. [49]

<sup>1</sup>H-NMR (300 MHz, CDCl<sub>3</sub>),  $\delta$  (ppm): 7.31 (s, 2H), 2.58 (d,  $J$  = 7.2 Hz, 4H), 1.73-1.60 (2H), 1.36-1.21 (16H), 0.92-0.84 (12H).

**M5:** [50] Bromine (1.51 mL, 29.1 mmol) was added dropwise in the dark to a mixture of 1,4-bis(2-ethylhexyl)benzene (12, 3.83 g, 12.7 mmol) and iodine (32.8 mg, 129  $\mu$ mol) at 0 °C. The mixture was stirred for 48 h at room temperature. After that time, 20 mL of DCM and 20 mL of NaOH (20%) were added and the phases were separated. The aqueous phase was extracted with DCM (2 x 20 mL) and the combined organic phases were washed with 60 mL of NaOH (20%), Na<sub>2</sub>S<sub>2</sub>O<sub>3</sub> (2 x 60 mL) and brine (1 x 60 mL), dried over Na<sub>2</sub>SO<sub>4</sub> and concentrated under reduced pressure. The crude product was purified by flash column chromatography using hexane as eluent to afford compound M5 as a colourless oil (3.43 g, 58%)

<sup>1</sup>H-NMR (300 MHz, CDCl<sub>3</sub>),  $\delta$  (ppm): 7.31 (s, 2H), 2.58 (d,  $J$  = 7.2 Hz, 4H), 1.73-1.60 (2H), 1.36-1.21 (16H), 0.92-0.84 (12H).

**M6:** [30] 1,4,4,8-Naphthalenetetracarboxylic dianhydride (2.70 g, 9.99 mmol) was suspended in 25 mL of H<sub>2</sub>SO<sub>4</sub> (96%) and the mixture was stirred for 5 min. Next, 1,3-dibromo-5,5-dimethylhydantoin (DBDMH, 4.28 g, 15.0 mmol) was added to the mixture in portions over a period of 1 h at room temperature. The reaction mixture was then stirred during 48 h at 50 °C. After that time, the mixture was poured into crushed ice and the precipitated solid was filtered and washed several times with water.

Finally, the yellow product was dried in vacuum (3.80 g, 89%), which was used directly in the next step without further purification.

<sup>1</sup>H-NMR (300 MHz, DMSO),  $\delta$  (ppm): 8.79 (s, 2H).

**P0:** In a Schlenk flask three cycles of argon-vacuum were applied. Next, monomer M6 (549 mg, 721  $\mu$ mol), monomer M4 (400 mg, 721  $\mu$ mol), NaHCO<sub>3</sub> (2.42 g, 28.8 mmol) and Pd(PPh<sub>3</sub>)<sub>4</sub> (16.7 mg, 14.4  $\mu$ mol) were dissolved in 10 mL of a mixture of THF:water (8:3) previously degassed. The reaction mixture was stirred and refluxed for 6 d. After that, 30 mL of chloroform and 30 mL of water were added to the mixture and the phases were separated. The aqueous phase was extracted with chloroform (2 x 30 mL) and the combined organic phases were washed with brine (1 x 100 mL), dried over Na<sub>2</sub>SO<sub>4</sub> and the solvent removed under reduced pressure. The crude product was dissolved in 0.7 mL of chloroform and dripped into 200 mL of MeOH. The orange precipitate was filtered off and washed with MeOH (4 d), acetone (3 d) and CH<sub>3</sub>CN (3 d) using a Soxhlet extractor to afford P0 (90.7 mg, 14%). SEC:  $M_n$  = 4350,  $M_w$  = 6953, PDI = 1.6.

<sup>1</sup>H-NMR (300 MHz, CD<sub>2</sub>Cl<sub>2</sub>),  $\delta$  (ppm): 8.82 (s, 2H), 7.18 (s, 2H), 4.49-3.82 (4H), 2.68-2.22 (16H), 2.02-1.71 (4H), 1.69-1.52 (2H), 1.52-1.28 (16H), 1.18-0.80 (28H), 0.77-0.55 (12H).

MS (MALDI-TOF): The building block (C<sub>58</sub>H<sub>86</sub>N<sub>4</sub>O<sub>4</sub> [M]<sup>+</sup>: 902.664) of P0 was detected. (Figure S5)

**P1:** Copolymer P0 (130 mg, 144  $\mu$ mol) was dissolved in 2 mL of THF. Next, iodoethane (690  $\mu$ L, 8.64 mmol) and 1 mL of DMF were added, and the solution was stirred for 5 d at room temperature in darkness. After that, the reaction was put into water and the resulting precipitate was filtered and washed with AcOEt for 1 d using a Soxhlet extractor. The solid was dissolved in DCM and the remained solid was filtered off. The filtrate was evaporated under reduced pressure to give polymer P1 as an orange solid (100 mg, 57%).

<sup>1</sup>H-NMR (300 MHz, CD<sub>2</sub>Cl<sub>2</sub>),  $\delta$  (ppm): 8.97-8.60 (2H), 7.42-7.10 (2H), 4.52-4.05 (4H), 3.74-2.76 (16H), 2.61-2.12 (4H), 1.91-1.68 (6H), 1.56-1.33 (16H), 1.18-0.78 (34H), 0.78-0.48 (12H).

#### Perovskite Solution Preparation

580.0 mg of PbI<sub>2</sub> and 200.0 mg of MAI were dissolved in 0.7 mL of DMF and 0.3 mL of DMSO. The solution was stirred in a glove box at 70 °C for 12 h and then filtered using a 0.22  $\mu$ m PTFE syringe filter.

#### Device Fabrication

The FTO/glass substrate was cleaned by successive sonication in detergent (2% Hellmanex water solution), deionized water, isopropyl alcohol and ethanol for 20 min and then dried by flowing dry oxygen. After a 30 min UV-ozone treatment, 100  $\mu$ L of the NiO<sub>x</sub> precursor solution (25.4 mg ml<sup>-1</sup> Ni(OAc)<sub>2</sub>·4H<sub>2</sub>O in 2-methoxyethanol and 6.04  $\mu$ L of ethanolamine) was spread over an FTO substrate and spin coated for 40 s at 4000 rpm with a ramp of 2000 rpm s<sup>-1</sup>. The substrates were immediately annealed at 300 °C for 10 min and followed by 500 °C for 30 minutes in air. For the deposition of perovskite films and further processing, the substrates were transferred into a glove box. 70  $\mu$ L of perovskite solution was deposited on top of the NiO<sub>x</sub> layer by a two-step spin-coating process at 1000 rpm with a ramp of 200 rpm s<sup>-1</sup> and 4000 rpm with a ramp of 3000 rpm s<sup>-1</sup> for 5 and 45 s, respectively. During the spinning, 200  $\mu$ L of chlorobenzene were dropped on the middle of the film 35 s before the end of the procedure. The substrates were then annealed at 60 °C for 1 min and then 100 °C for 10 min. 50  $\mu$ L of the PC<sub>61</sub>BM solution (20 mg ml<sup>-1</sup> in chlorobenzene) was dynamically spun onto the perovskite layer at 2000 rpm for 45 s with acceleration of 1000 rpm s<sup>-1</sup>, then annealed at 100 °C for 10 min. For the buffer layer, BCP was fully dissolved in EtOH, P0 in EtOAc:MeOH (1:1), M1 and P1 in MeOH to concentration of 1 mg ml<sup>-1</sup>. 50  $\mu$ L of each buffer solution was dynamically spin-coated on top of PC<sub>61</sub>BM layer at 4000 rpm for 30 s with a ramp of 2000 rpm s<sup>-1</sup>.

## Acknowledgements

A. C.-E. and S. C. acknowledge the Polymat Foundation for a PhD and a Postdoctoral research position, respectively. J. L. D. acknowledges Ikerbasque, the Basque Foundation for Science, for an "Ikerbasque Research Fellow" contract, the Polymat Foundation and the MINECO of Spain for CTQ 2016-81911-REDT and RTI2018-101782-B-I00 grants.

**Keywords:** Naphthalene Diimides • Perovskite Solar Cells • PC<sub>61</sub>BM • Buffer Layer • Stability

- [1] A. Kojima, K. Teshima, Y. Shirai, and T. Miyasaka, *J. Am. Chem. Soc.*, **2009**, *131*, 6050-6051.
- [2] NREL, Best Research-Cell Efficiencies Chart, <https://www.nrel.gov/pv/assets/pdfs/best-research-cell-efficiencies.20191104.pdf>.
- [3] S. F. Völker, S. Collavini, and J. L. Delgado, *ChemSusChem*, **2015**, *8*, 3012-3028.
- [4] J. Urieta-Mora, I. García-Benito, A. Molina-Ontoria, and N. Martín, *Chem. Soc. Rev.*, **2018**, *47*, 8541-8571.
- [5] S. Collavini and J. L. Delgado, *Sustainable Energy Fuels*, **2018**, *2*, 2480-2493.
- [6] S. Sun, T. Buonassisi, and J.-P. Correa-Baena, *Adv. Mater. Interfaces*, **2018**, *5*, 1800408.
- [7] J. Lian, B. Lu, F. Niu, P. Zeng, and X. Zhan, *Small Methods*, **2018**, *2*, 1800082.
- [8] T. Gatti, E. Menna, M. Meneghetti, M. Maggini, A. Petrozza, and F. Lamberti, *Nano Energy*, **2017**, *41*, 84-100.
- [9] E. Castro, J. Murillo, O. Fernandez-Delgado, and L. Echegoyen, *J. Mater. Chem. C*, **2018**, *6*, 2635-2651.
- [10] J. C. Hummelen, B. W. Knight, F. LePeq, F. Wudl, J. Yao, and C. L. Wilkins, *J. Org. Chem.*, **1995**, *60*, 532-538.
- [11] J.-Y. Jeng, Y.-F. Chiang, M.-H. Lee, S.-R. Peng, T.-F. Guo, P. Chen, and T.-C. Wen, *Adv. Mater.*, **2013**, *25*, 3727-3732.
- [12] D. Luo, W. Yang, Z. Wang, A. Sadhanala, Q. Hu, R. Su, R. Shivanna, G. F. Trindade, J. F. Watts, Z. Xu, T. Liu, K. Chen, F. Ye, P. Wu, L. Zhao, J. Wu, Y. Tu, Y. Zhang, X. Yang, W. Zhang, R. H. Friend, Q. Gong, H. J. Snaith, and R. Zhu, *Science*, **2018**, *360*, 1442.
- [13] J. K. Mwaure, M. R. Pinto, D. Witker, N. Ananthakrishnan, K. S. Schanze, and J. R. Reynolds, *Langmuir*, **2005**, *21*, 10119-10126.
- [14] W. Zhao, S. Li, H. Yao, S. Zhang, Y. Zhang, B. Yang, and J. Hou, *J. Am. Chem. Soc.*, **2017**, *139*, 7148-7151.
- [15] J. Seo, S. Park, Y. Chan Kim, N. J. Jeon, J. H. Noh, S. C. Yoon, and S. I. Seok, *Energy Environ. Sci.*, **2014**, *7*, 2642-2646.
- [16] M. Al Kobaisi, S. V. Bhosale, K. Latham, A. M. Raynor, and S. V. Bhosale, *Chem. Rev.*, **2016**, *116*, 11685-11796.
- [17] X. Zhan, A. Facchetti, S. Barlow, T. J. Marks, M. A. Ratner, M. R. Wasielewski, and S. R. Marder, *Adv. Mater.*, **2011**, *23*, 268-284.
- [18] J. H. Heo, S.-C. Lee, S.-K. Jung, O. P. Kwon, and S. H. Im, *J. Mater. Chem. A*, **2017**, *5*, 20615-20622.
- [19] S. K. Jung, J. H. Heo, D. W. Lee, S. H. Lee, S. C. Lee, W. Yoon, H. Yun, D. Kim, J. H. Kim, S. H. Im, and O. P. Kwon, *ChemSusChem*, **2019**, *12*, 224-230.
- [20] S. K. Jung, J. H. Heo, D. W. Lee, S. C. Lee, S. H. Lee, W. Yoon, H. Yun, S. H. Im, J. H. Kim, and O. P. Kwon, *Adv. Funct. Mater.*, **2018**, *28*, 1800346.
- [21] T. Nakamura, N. Shiota, T. Shimoaka, R. Nishikubo, T. Hasegawa, A. Saeki, Y. Murata, R. Murdey, and A. Wakamiya, *Chem. Mater.*, **2019**, *31*, 1729-1737.
- [22] S.-K. Jung, J. H. Heo, B. M. Oh, J. B. Lee, S.-H. Park, W. Yoon, Y. Song, H. Yun, J. H. Kim, S. H. Im, and O. P. Kwon, *Adv. Funct. Mater.*, **2020**, *30*, 1905951.
- [23] W. Wang, J. Yuan, G. Shi, X. Zhu, S. Shi, Z. Liu, L. Han, H.-Q. Wang, and W. Ma, *ACS Appl. Mater. Interfaces*, **2015**, *7*, 3994-3999.
- [24] S. Shao, Z. Chen, H. H. Fang, G. H. ten Brink, D. Bartesaghi, S. Adjokatse, L. J. A. Koster, B. J. Kooi, A. Facchetti, and M. A. Loi, *J. Mater. Chem. A*, **2016**, *4*, 2419-2426.
- [25] C. Sun, Z. Wu, H.-L. Yip, H. Zhang, X.-F. Jiang, Q. Xue, Z. Hu, Z. Hu, Y. Shen, M. Wang, F. Huang, and Y. Cao, *Adv. Energy Mater.*, **2016**, *6*, 1501534.
- [26] J. H. Heo, D. S. Lee, D. H. Shin, and S. H. Im, *J. Mater. Chem. A*, **2019**, *7*, 888-900.
- [27] X. Zheng, B. Chen, J. Dai, Y. Fang, Y. Bai, Y. Lin, H. Wei, Xiao C. Zeng, and J. Huang, *Nat. Energy*, **2017**, *2*, 17102.
- [28] Z. Wu, C. Sun, S. Dong, X.-F. Jiang, S. Wu, H. Wu, H.-L. Yip, F. Huang, and Y. Cao, *J. Am. Chem. Soc.*, **2016**, *138*, 2004-2013.
- [29] B. Russ, M. J. Robb, B. C. Popere, E. E. Perry, C.-K. Mai, S. L. Fronk, S. N. Patel, T. E. Mates, G. C. Bazan, J. J. Urban, M. L. Chabiny, C. J. Hawker, and R. A. Segalman, *Chem. Sci.*, **2016**, *7*, 1914-1919.
- [30] M. Sasikumar, Y. V. Suseela, and T. Govindaraju, *Asian J. Org. Chem.*, **2013**, *2*, 779-785.
- [31] L. Li, *MALDI MS: A Practical Guide to Instrumentation, Methods and Applications (Ed: Franz Hillenkamp and Jasna Peter - Katalinić)*, **2007**, 245-297.
- [32] P. M. Alvey, R. J. Ono, C. W. Bielawski, and B. L. Iverson, *Macromolecules*, **2013**, *46*, 718-726.
- [33] N. B. Kolhe, A. Z. Ashar, K. S. Narayan, and S. K. Asha, *Macromolecules*, **2014**, *47*, 2296-2305.
- [34] S. Vasimalla, S. P. Senanayak, M. Sharma, K. S. Narayan, and P. K. Iyer, *Chem. Mater.*, **2014**, *26*, 4030-4037.
- [35] P. M. Alvey and B. L. Iverson, *Org. Lett.*, **2012**, *14*, 2706-2709.
- [36] H. Huang, N. Zhou, R. P. Ortiz, Z. Chen, S. Loser, S. Zhang, X. Guo, J. Casado, J. T. López Navarrete, X. Yu, A. Facchetti, and T. J. Marks, *Adv. Funct. Mater.*, **2014**, *24*, 2782-2793.
- [37] A. Luzio, D. Fazzi, D. Natali, E. Giussani, K.-J. Baeg, Z. Chen, Y.-Y. Noh, A. Facchetti, and M. Caironi, *Adv. Funct. Mater.*, **2014**, *24*, 1151-1162.
- [38] Y. Kim, J. Hong, J. H. Oh, and C. Yang, *Chem. Mater.*, **2013**, *25*, 3251-3259.
- [39] F. Doria, I. Manet, V. Grande, S. Monti, and M. Freccero, *J. Org. Chem.*, **2013**, *78*, 8065-8073.
- [40] H. Chen, Y. Guo, Z. Mao, G. Yu, J. Huang, Y. Zhao, and Y. Liu, *Chem. Mater.*, **2013**, *25*, 3589-3596.
- [41] T. Jia, C. Sun, R. Xu, Z. Chen, Q. Yin, Y. Jin, H.-L. Yip, F. Huang, and Y. Cao, *ACS Appl. Mater. Interfaces*, **2017**, *9*, 36070-36081.
- [42] B. L. Schottel, H. T. Chifotides, and K. R. Dunbar, *Chem. Soc. Rev.*, **2008**, *37*, 68-83.
- [43] Q. Song, F. Li, Z. Wang, and X. Zhang, *Chem. Sci.*, **2015**, *6*, 3342-3346.
- [44] C. Duan, W. Cai, B. B. Y. Hsu, C. Zhong, K. Zhang, C. Liu, Z. Hu, F. Huang, G. C. Bazan, A. J. Heeger, and Y. Cao, *Energy Environ. Sci.*, **2013**, *6*, 3022-3034.
- [45] C.-C. Chueh, C.-Z. Li, and A. K. Y. Jen, *Energy Environ. Sci.*, **2015**, *8*, 1160-1189.
- [46] F. Huang, L. Hou, H. Wu, X. Wang, H. Shen, W. Cao, W. Yang, and Y. Cao, *J. Am. Chem. Soc.*, **2004**, *126*, 9845-9853.
- [47] P. B. Balanda, M. B. Ramey, and J. R. Reynolds, *Macromolecules*, **1999**, *32*, 3970-3978.
- [48] C. M. Cardona, W. Li, A. E. Kaifer, D. Stockdale, and G. C. Bazan, *Adv. Mater.*, **2011**, *23*, 2367-2371.
- [49] T. Schwalm and M. Rehahn, *Macromolecules*, **2007**, *40*, 3921-3928.
- [50] P. Wessig, M. Gerngroß, D. Freyse, P. Bruhns, M. Przewdzia, U. Schilde, and A. Kelling, *J. Org. Chem.*, **2016**, *81*, 1125-1136.

## Naphthalene Diimide-Based Molecules for Efficient and Stable Perovskite Solar Cells



### Key Topic: Polymers as Additives for Perovskite Solar Cells

Naphthalene Diimides (NDI) are promising candidates to improve the performances and the stability of perovskite solar cells. In this paper, three novel NDI-based molecules are synthesized, characterized, and incorporated into solar devices as buffer layers between the electron transporting layer and the cathode. The evaluation of the performances and of the stability of the cells highlighted the beneficial effects brought by these molecules.

Institute and/or researcher Twitter usernames:

@bercpolymat

@upvehu

@JuanLDelgadoC